Biocompatibility of silicon nanowires: A step towards IC detectors

Cite as: AIP Conference Proceedings **2145**, 020011 (2019); https://doi.org/10.1063/1.5123572
Published Online: 27 August 2019

Paola Piedimonte, Sergio Fucile, Cristina Limatola, Massimiliano Renzi, and Fabrizio Palma

Biocompatibility of Silicon NanoWires: A Step Towards IC Detectors

Paola Piedimonte[1], Sergio Fucile[2, 3], Cristina Limatola[2], Massimiliano Renzi[2, a)] Fabrizio Palma[1, b)]

[1]*Department SBAI, Sapienza University of Rome, Via Scarpa 14, 00184 Rome, Italy*
[2]*Department of Physiology and Pharmacology, Sapienza University of Rome, P.le A. Moro 5, 00184 Rome, Italy*
[3]*IRCCS Neuromed, Pozzilli, Italy*

[a)] Corresponding author: massimiliano.renzi@uniroma1.it
[b)] fabrizio.palma@uniroma1.it

Abstract. Recording bioelectric signals at high spatio-temporal resolution with low invasiveness is a major challenge in the field of bio-nanotechnology. Insofar, bioactive signals have been recorded with improved signal-to-noise ratio from cells in culture using arrays of nanopillars. However, production of such nanoscale electrodes is both time-consuming, pricey and might be only scarcely compatible with the Complementary Metal-Oxide-Semiconductor integrated circuits (CMOS-IC) technology. To take a step forward, we introduced an innovative approach to fabricate small, high-density Silicon NanoWires (SiNWs) with a fast, relatively inexpensive and low-temperature (200 °C) method. Growth of such SiNWs is compatible with ICs, thus theoretically allowing on-site amplification of bioelectric signals from living cells in tight contact. Here, we report our preliminary results showing biocompatibility and neutrality of SiNWs used as seeding substrate for cells in culture. With this technology, we aim to produce a compact device allowing on-site, synched and high signal/noise recordings of a large amounts of biological signals from networks of excitable cells (e.g. neurons) or from different areas of a single cell surface, thus providing super-resolved descriptions of bioelectric waveforms at the microdomain level.

INTRODUCTION

Ionic currents across membranes are crucial in both excitable and non-excitable cells and their accurate measurement requires efficient coupling between cell membrane and recording electrode. An elective approach to investigate membrane currents and potentials, from network to single-channel level, is the patch-clamp technique [1]. However, in most configurations patch-clamp relies on accessing (thus, perturbing) the interior of single cells, which limits the recording output both in duration and overall number of examined samples. Extracellular recording methods, such as multi-electrode arrays (MEA) [2] and multi-transistor arrays [3], are noninvasive and allow for long-lasting, multiplexed measurements. However, these methods not only sacrifice the one-to-one correspondence between cells and electrodes, but also might provide recordings with reduced signal resolution. A valid alternative is represented by optical methods based on ion indicators and voltage-sensitive dyes [reviewed in 4]. These technologies can in fact deliver massively parallel recordings, yet they might still suffer for perfectible resolution and applicability. Overall, both high-resolution investigation of cell excitability and pharmacological screening of ion-channel drugs are still commonly performed using low-throughput, intracellular recording methods [reviewed in 5].

In this scenario, assembling an all-electrical device for electrophysiological imaging (that is, a closely packed MEA directly connected to a CMOS thus capable of high-precision intracellular recording from a large network of cells) has long been a major pursuit in bioengineering applied to neuro- and cardio- experimental physiology [6]. Importantly, a major challenge to this approach proved to be the electrical screening of biological signals along even very short distance (e.g. ~10 nm) between the 'source' and the 'detector' [7].

NANOINNOVATION 2018
AIP Conf. Proc. 2145, 020011-1–020011-7; https://doi.org/10.1063/1.5123572
Published by AIP Publishing. 978-0-7354-1890-5/$30.00

Recently, adoption of nanowire transistors [8] and nanotube-coupled transistors [9] did pave the way to a new technology with significantly improved signal resolution during recordings from living cells. Thus, nano-electrodes of various geometries connected to CMOS-ICs could be used to record action potentials from cardiomyocytes in culture over a long period of time with much improved signal resolution [10, 11]. Using such approach, it was possible to repeatedly switch between extracellular and intracellular recording by nanoscale electroporation/resealing processes and to detect subtle changes of the action potential waveform induced by ion channel drugs. CMOS-based MEAs have also been very recently combined to laser-induced opto-poration to allow for long-lasting, simultaneous extra- and intra-cellular recordings with good signal-to-noise ratio from mammalian neurons or cardiac-derived cells in culture [12]. However, nanopillar recording and CMOS-based microelectronics have not been combined insofar into an all-electrical, low-cost device due to the little compatibility between CMOS technology and the nanotechnology required to grow on site, small-sized, packed nanowires.

To fill this gap, we designed a new-generation, all-electrical array bearing two major points of strength. First, to acquire electrical signals at high resolution we use an image sensor consisting of a large-scale, high-density and high-sensitivity (6 el/sec) array integrated with CMOS electronics on a single chip. Secondly, to minimize the electrical screening of biological signals we have the Silicon NanoWires (SiNWs; used as nano-detectors) grown directly onto the ICs, thus providing an extremely tight coupling between the cell membrane and the recording device. By introducing such innovative technology we hope to overcome the limitations suffered insofar in the field and aim to produce a device for massively parallel electrophysiological imaging of biological samples at high-resolution.

MATERIALS AND METHODS

Deposition of Silicon NanoWires

SiNWs were grown on a Si substrate by Chemical Vapor Deposition (CVD) using a vapor-liquid-solid (VLS) reaction. The substrates used were all Floating Zone wafer 1Ω·cm, orientation <100>, 250 µm-thick. The semiconductor wafers were first cleaned with RCA solution (6 parts deionized H_2O, 1-part HCl 27% solution, 1-part H_2O_2 30% solution; 80 °C). At the end of the process, a silicon oxide passivation layer was laid on the silicon surface and in a separate chamber a 5 nm-thick layer of Sn was evaporated onto the silicon oxide layer.

To grow SiNWs, the substrate was baked at 400 °C in a vacuum chamber at 1×10^{-6} mbar pressure under a fast heating regime (3200 °C/h), so to ensure the formation of very small Sn droplets on the substrate surface. The temperature was measured using a thermocouple in contact with the backside of the sample holder (which we will insofar refer to as the 'crucible').

After slow cooling to 200 °C, the sample was exposed for 5 min to H_2 plasma at 600 W under a chamber pressure of 2 mbar and a gas flux of 50 sccm.

In the final step, the sample was processed for 4 min with SiH_4 at 300 W (in absence of plasma activation) with a chamber pressure of 2 mbar and a gas flux of 15 sccm.

Cell Cultures, Patch-Clamp and Ca^{2+} Imaging

Cell Cultures

NG108CC15 cells ('NG cells'; hybrid from mouse neuroblastoma N18TG2 and rat glioma C6BUI cells) were grown in standard conditions (37 ºC; 5% CO_2) using DMEM supplemented with 10% FBS, 100 U/ml penicillin, 0.1 mg/ml streptomycin (P/S), 100 mM Hypoxanthine, 10 mM Aminopterin, and 16 mM Thymidine. NG cells grown in such non-differentiating conditions appeared relatively depolarized and void of mature action potentials, as expected [13]. BV-2 microglial line cells were grown in 10% FBS, 1% P/S DMEM. All cells were plated on uncoated substrates (glass coverslips or SiNWs) and used 24-48 hrs after seeding.

Patch-Clamp and Ca^{2+} Imaging

For patch-clamp, cells were bathed with standard external solution containing (in mM): 145 NaCl, 2 $CaCl_2$, 1 or 2 $MgCl_2$, 4 KCl, 5 HEPES, 5 glucose, 2 Na-pyruvate (pH 7.4, NaOH). The 'intracellular' pipette solution contained (in mM): 110 K-gluconate, 12 KCl, 10 Na_2-Phosphocreatine, 10 HEPES, 0.1

EGTA, 4 Mg-ATP, 0.3 Na-GTP (pH 7.3, KOH; 295 mosm, adjusted with sucrose). The open-tip resistance of borosilicate pipettes ranged from 4.5 to 9.5 MΩ prior to 30~60% compensation. Due to the substrate opacity to transmitted light, cells on engineered substrates were visualized using IR-DIC optics (Leica DM LFS); recordings were acquired using pClamp9 controlling a MultiClamp 700B amplifier (Molecular Devices). In current-clamp experiments, to describe the passive and active properties of NG cells we applied a family of current steps (I_{inj} –200 to +600 pA, 50 pA increments, 1s-long; inter-sweep-interval 1.5 sec; HP –80 mV). Cell input resistance (R_{in}) was calculated as the slope of the linear least-squares fit to the voltage–steady state current relationship corresponding to the first four hyperpolarizing steps. Voltage-sag was estimated as the average percentage decrease of the $|V_m|$ at the steady-state vs peak response to the first three hyperpolarizing steps [14]. For voltage-clamp experiments, to investigate the expression of voltage-activated Inwardly Rectifying (IR) or Outwardly Rectifying (OR) K^+ channels BV-2 cells were challenged with a family of voltage steps (V_{cmd} –130 to +30 mV, 1-sec long, 20 mV/step, inter-sweep-interval 5 sec; HP –70 mV). The current density was calculated as current/whole-cell capacitance, the latter being estimated using the amplifier compensation circuit.

For Ca^{2+} imaging, cells were loaded with the Ca^{2+}-sensitive fluorescent dye Fura-2 (cell permeant, 2 μM; 45 min at 37 ºC) and recordings were performed in standard external solution (above). Control or agonist (1 mM ATP, 3-sec long application) solutions were delivered by independent tubes positioned 50–100 μm away from the cell and connected to a fast exchanger system (RSC 100, Biologic). Epifluorescence acquisition was driven by Axon Imaging Workbench software (Molecular Devices; 380 nm exc. and 510 nm em. wavelength).

All recordings were at room temperature. Results are shown as mean ± SEM; unpaired *t*-tests were used when possible.

RESULTS AND DISCUSSION

NanoWires Can Be Grown on Silicon Substrates

Our first step was to grow nanowires on silicon substrate using the Microwawes Chemical Vapor Deposition (MWCVD) system. The deposition chamber (Fig. 1) consists of a cylindrical tube allowing for the propagation of only the first TE 10 mode of the microwaves field generated by a magnetron at 2.5 GHz and injected into the chamber by an antenna structure. A quartz disc allows for the passage of microwaves while ensuring the preservation of high vacuum in the chamber. The bottom of the chamber consists of a sample holder (the crucible, stainless still or graphite), which serves as substrate induction heater and is fed by a 100 KHz power controller. The position of the crucible can be controlled on the z-axis so to adjust the waveguide conditions. A dielectric spacer is positioned between the surface of the crucible and the sample substrate both to damp the intensity of the tangential electric field of the microwaves and to avoid energy dissipation onto the conducting crucible, rather than onto the Si surface. SiNWs are grown as the result of heating the Si substrate in presence of a thin metal layer: the metal droplets formed do function as nano-susceptors of nanowires which in turn build-up in presence of inflowing SiH_4 gas once the eutectic temperature is overcome. The choice of the metal catalyst is key in our deposition method. Au has long been the metal of choice to grow Si wires and still is the most frequently used catalyst [15-17]. However, in recent years efforts have been made to find a valid alternative, as using Au induces deep level defects in the Si structure [18], thus making this catalyst scarcely compatible with the CMOS technology standards.

We chose Sn as catalysts material for its full compatibility with the innovative fabrication method adopted, that is nanowire deposition at low-temperature and on-site growth on CMOS-ICs [19].

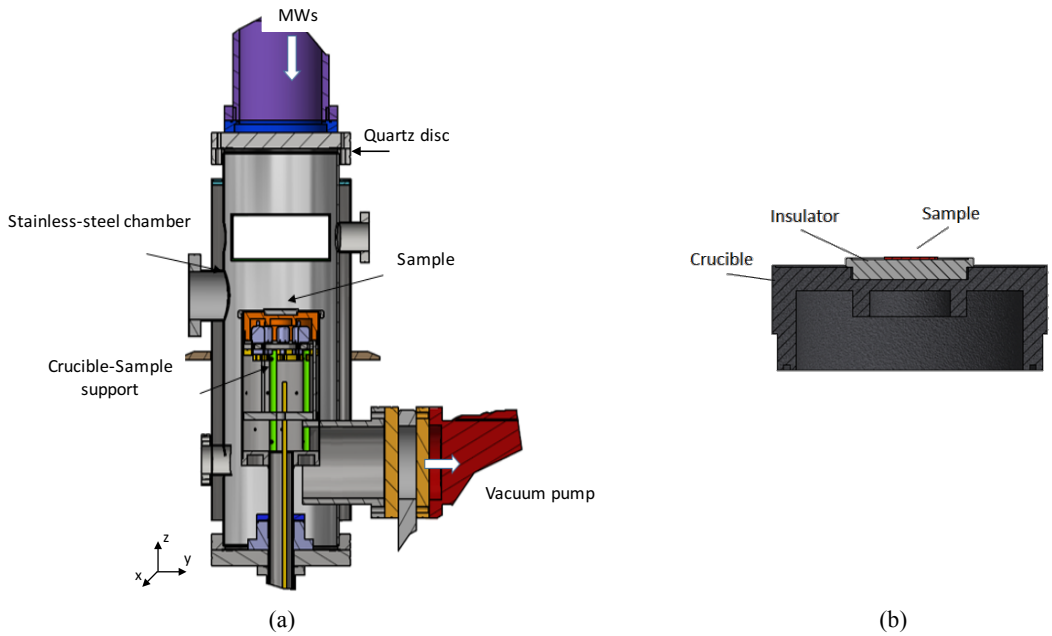

FIGURE 1. Schematic of the MWCVD deposition chamber (a) and the crucible for substrate heating (b). The sample is located on the crucible support bearing a dielectric spacer between the sample and the conductive plane. Because of the tangential electric field concentrated on the sample, Sn droplets are heated up by MWs and work as nano-susceptors.

In particular, the phase diagram of the Silicon-Tin system shows a point of eutectic very close to the melting point of pure tin, to the far right of the diagram (5×10^{-5} at.% of Si and 1×10^{-4} °C below the Sn melting point; [20]). Along the deposition process, thanks to the MW irradiation, Sn nano-susceptors do overcome the eutectic temperature and trigger the VLS reaction to grow SiNWs even in presence of a limited percentage of SiH_4 and a relatively low substrate temperature (200 °C).

The procedure described leads to the deposition on the silicon substrate of SiNWs with the desired size (typically ~20 nm diameter) and spacing, within some variability (Fig. 2).

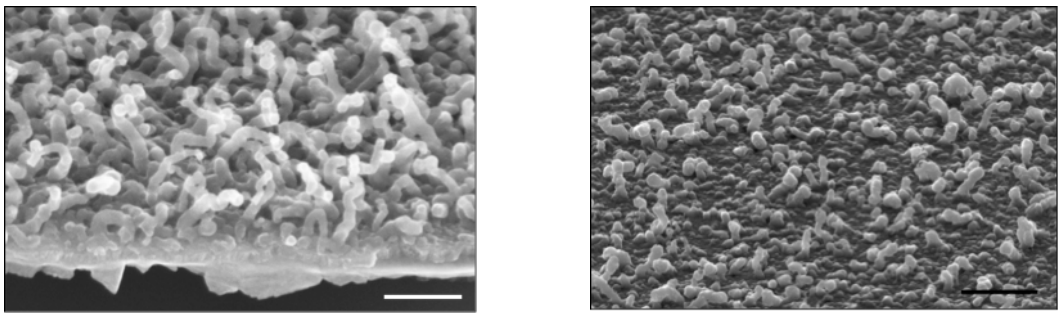

FIGURE 2. SEM images of typical SiNWs with cross section ~20 nm (a, silicon; b, silicon oxide) grown using the MWCVD method and tested as 'substrates' for cell cultures and physiological recordings. Note the Sn droplets still evident at nanowire tips. Scale bar: 100 nm.

NanoWires on Silicon Substrates Are Bio-Compatible

As we succeed growing nanowires on silicon substrates, our obvious next step was testing their biocompatibility. Bearing in mind the possible application of our engineered substrates as components for both high-resolution recording devices and conditioning prosthetic implants, we chose to investigate the effects of SiNWs on neuronal and microglial cells to start with. Thus, we used

NG108CC15 cells, a hybrid cell line showing some neuronal properties [13]; and BV-2 cells, a murine cell line commonly chosen to model native microglia [21, 22]. We also tested SiNWs for biocompatibility using primary cultures from neonatal mice and verified that both hippocampal neurons and microglial cells can be grown on SiNWs with no alteration of their morphology (immunofluorescence preliminary data; not shown). Notably, all cell types tested were successfully grown on engineered substrates. In particular, in current-clamp experiments we found that in response to the injection of hyperpolarizing and depolarizing current steps NG cells had both passive properties (resting membrane potential; membrane capacitance; voltage sag and input resistance) and active response (firing profile) unaltered by the presence of SiNWs as seeding substrate (Fig. 3, a). Likewise, when investigating BV-2 cells in voltage-clamp experiments to test for their membrane expression of voltage-activated IR or OR K^+ channels [23], we found no difference across seeding conditions (Fig. 3, b). To further demonstrate that cells grown on SiNWs do express a pattern of membrane receptors similar to those present in physiological conditions we performed Ca^{2+} imaging experiments on BV-2 cells on SiNWs and found that both basal intracellular [Ca^{2+}] and 1 mM ATP-elicited [Ca^{2+}]$_i$ rise were typical of these cells in normal culture conditions (Fig. 4; [24]). Altogether, our preliminary investigations indicate that SiNWs do not alter normal survival and basic properties of both microglial and neuronal cells *in vitro* thus resulting amenable for non-interfered biological measures.

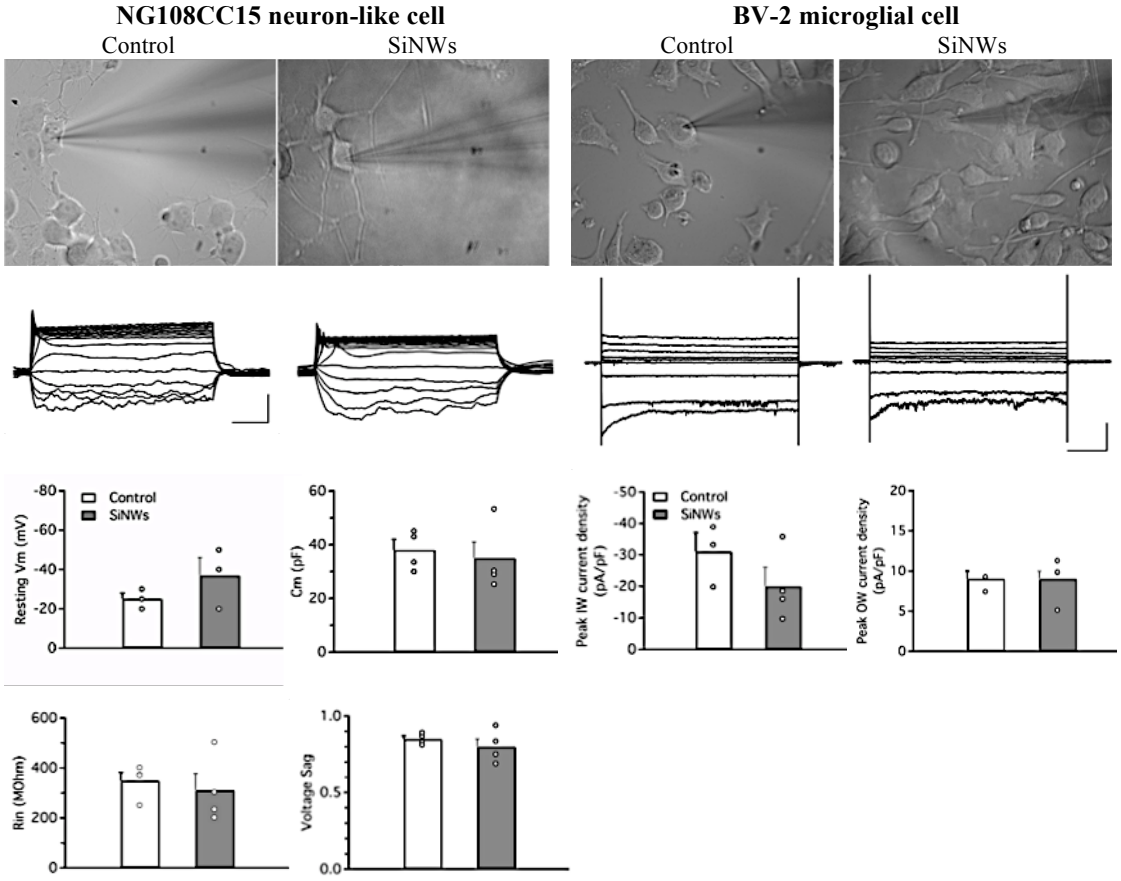

FIGURE 3. Patch-clamp recording from cells in culture on uncoated glass coverslips (Control) or silicon nanowires (SiNWs). (a), current-clamp experiments on NG108CC15 cells. Cells show i) unaltered morphology under IR-DIC visualization (upper panels); ii) similar firing profile typical of NG cells kept in non-differentiating culture condition (i.e., lack of spike trains in response to depolarizing injected currents; middle panels); and iii) similar passive properties (bar plots in lower panels; p>0.3 or more, unpaired t-test when applicable). (b), voltage-clamp experiments on BV-2 cells. Panels depict lack of difference across seeding substrates for both cell morphology and peak current density. Note that transmitted light images captured in presence of SiNWs appear blurry due to the optical properties of silicon substrates. Scale bars: current-clamp, 100 ms, 20 mV; voltage-clamp, 200 ms, 200 pA.

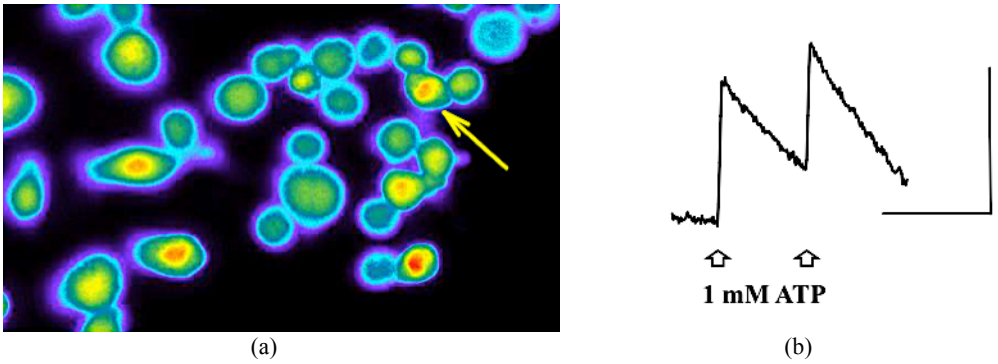

(a) (b)

FIGURE 4. Ca^{2+} imaging experiments from BV-2 cells in culture on SiNWs. (a), typical optic field depicting fura-2 AM loaded cells. The arrow indicates a cell responsive to the fast application of 1 mM ATP. (b), time course of the fluorescence response (indicating $[Ca^{2+}_i]$ rise) to two consecutive applications of ATP (arrows). Typically, we found three-to-four responsive cells per optical field (6 fields analysed across different substrates, no difference found). Bars: fluorescence ratio 0.05; 100 s.

CONCLUSIONS

We described a novel technology for the fabrication of small, high-density Silicon NanoWires, which can theoretically be grown directly on CMOS IC-equipped substrates. Our method is fast, inexpensive and works at relatively low temperature.

SiNWs are neutral to living cells and thus potentially amenable to pass electric signals both from and onto cells in tight contact. We are now testing such potential, aiming to produce a compact, all-electrical device for highly resolved cell recording/conditioning.

ACKNOWLEDGMENTS

We thank Dr Francesco Mura for his invaluable help with SEM images and Dr Giuseppina D'Alessandro for immunofluorescence preliminary data.

REFERENCES

[1] B. Sakmann and E. Neher, *Single-channel recording* (Springer, New York, 1995).
[2] J. Pine, J. Neurosci. Methods **2**(1), 19–31 (1980).
[3] W. Gindl, H. S. Gupta, T. Schöberl, H. C. Lichtenegger and P. Fratz, Applied Physics A **79**(8), 2069–2073 (2004).
[4] D. S. Peterka, H. Takahashi and R. Yuste, Neuron **69**(1), 9–21 (2011).
[5] A. Obergrussberger, S. Stölzle-Feix, N. Becker, A. Brüggemann, N. Fertig and C. Möller, Channels (Austin) **9**(6), 367–375 (2015).
[6] P. Fromherz, Chem. Phys. Chem. **3**(3), 276–284 (2002).
[7] E. R. Fossum and D. B. Hondongwa, IEEE J. Electron Devices Soc. **2**(3), 33–43 (2014).
[8] B. P. Timko, T. Cohen-Karni, G. Yu, Q. Qin, B. Tian and C. M. Lieber, Nano Letters, **9**(2), 914–918 (2009).
[9] X. Duan, R. Gao, P. Xie, T. Cohen-Karni, Q. Qing, H. S. Choe, B. Tian, X. Jiang and C. M. Lieber, Nature Nanotechnology **7**(3), 174–179 (2011).
[10] C. Xie, Z. Lin, L. Hanson, Y. Cui and B. Cui, Nature Nanotechnology **7**(3), 185–190 (2012).
[11] J. Abbott, T. Ye, L. Qin, M. Jorgolli, R. S. Gertner, D. Ham and H. Park, Nature nanotechnology **12**(5), 460–466 (2017).
[12] M. Dipalo, H. Amin, L. Lovato, F. Moia, V. Caprettini, G. C. Messina, F. Tantussi, L. Berdondini and F. De Angelis, Nano Letters **17**(6), 3932–3939 (2017).
[13] J. Liu, H. Tu, D. Zhang, H. Zheng and Y. L. Li, BMC Neuroscience **13**(129) (2012).

[14] B. A. Suter, M. Migliore and G. M. G. Shepherd, Cerebral Cortex **23**(8), 1965–1977 (2013).
[15] R. S. Wagner and W. C. Ellis, Applied Physics Letters **4**(5), 89–90 (1964).
[16] W. Chen, P. Pareige, C. Castro, T. Xu, B. Grandidier, D. Stiévenard and P. R. i Cabarrocas, Journal of Applied Physics **118**(10), 104301 (2015).
[17] A. Convertino, V. Mussi and L. Maiolo, Scientific Reports **6**, 25009 (2016).
[18] J. E. Allen, E. R. Hemesath, D. E. Perea, J. L. Lensch-Falk, Z. Y. Li, F. Yin, M. H. Gass, P. Wang, A. L. Bleloch, R. E. Palmer and L. J. Lauhon, Nature Nanotechnology **3**(3), 168–173 (2008).
[19] B. V. Schmidt, J. V. Wittemann, S. Senz, and U. Go, Advanced Materials **21**, 2681–2702 (2009).
[20] R. W. Olesinski and G. J. Abbaschian, Bulletin of Alloy Phase Diagrams **5**, 273–276 (1984).
[21] F. Li, J. Lu, C. Y. Wu, C. Kaur, V. Sivakumar, J. Sun, S. Li and E. A. Ling, J. Neurochem. **106**(5), 2093–2105 (2008).
[22] S. Rangaraju1, S. A. Raza, A. Pennati, Q. Deng, E. B. Dammer, D. Duong, M. W. Pennington, M. G. Tansey, J. J. Lah, R. Betarbet, N. T. Seyfried and A. I. Levey, Journal of Neuroinflammation **14**(1):128 (2017)
[23] S. Visentin, M. Renzi and G. Levi, GLIA **33**(3), 181–190 (2001).
[24] L. P. Bernier, A. R. Ase, S. Chevallier, D. Blais, Q. Zhao, E. Boué-Grabot, D. Logothetis and P. Séguéla, J. Neuroscience **28**(48), 12938–12945 (2008).